The 2006 Eruption of Augustine Volcano, Alaska
Power, J.A., Coombs, M.L., and Freymueller, J.T., editors
U.S. Geological Survey Professional Paper 1769

Chapter 14

Preliminary Slope-Stability Analysis of Augustine Volcano

By Mark E. Reid[1], Dianne L. Brien[1], and Christopher F. Waythomas[2]

Abstract

Augustine Volcano has been a prolific producer of large debris avalanches during the Holocene. Originating as landslides from the steep upper edifice, these avalanches typically slide into the surrounding ocean. At least one debris avalanche that occurred in 1883 during an eruption initiated a far-traveled tsunami. The possible occurrence of another edifice collapse and ensuing tsunami was a concern during the 2006 eruption of Augustine. To aid in hazard assessments, we have evaluated the slope stability of Augustine's edifice, using a quasi-three-dimensional, geotechnically based slope-stability model implemented in the computer program SCOOPS. We analyzed the effects of topography, variations in rock strength, and earthquake-induced strong ground motion on the relative stability of millions of potential large (>0.1 km^3 volume) slope failures throughout the edifice.

Preliminary results from pre-2006 topography provide three insights. First, the predicted stability of all parts of the upper edifice is approximately the same, suggesting an equal likelihood of slope failure, in agreement with geologic observations that debris avalanches have swept all sectors of the volcano. Second, the least stable (by a small amount) sector is on the east flank where a debris avalanche would flow into deeper ocean water and a resulting tsunami would be directed toward the southwestern part of the Kenai Peninsula. Third, most model scenarios predict stable edifice slopes, and only scenarios assuming extensive weak rocks and moderate to strong ground shaking predict potential large collapses. Because other transient triggering mechanisms, such as shallow magma intrusion, may be needed to instigate slope instability, monitoring ground deformation and seismicity could help short-term forecasting of impending edifice failure.

[1]U.S. Geological Survey, 345 Middlefield Road, MS 910, Menlo Park, CA 94025.

[2]Alaska Volcano Observatory, U.S. Geological Survey, 4200 University Drive, Anchorage, AK 99508.

Introduction

Augustine Volcano, an island volcano near the mouth of Cook Inlet, Alaska (fig. 1) composed primarily of multiple lava domes, has produced a remarkable series of large debris avalanches over the past 3,500 years. These debris avalanches, believed to initiate as massive landslides emanating from the flanks or summit of the edifice (Siebert and others, 1989; Begét and Kienle, 1992; Siebert and others, 1995), typically travel into the surrounding ocean (Waythomas and Waitt, 1998; Waythomas and others, 2006). Previous investigators have hypothesized that tsunamis occur when debris avalanches enter the sea during eruptions of the volcano (Kienle and Swanson, 1985; Kienle and others, 1987; Begét and Kienle, 1992; Siebert and others, 1995; Begét and Kowalik, 2006; Begét and others, 2008). A debris avalanche generated during the 1883 eruption of Augustine is believed to have caused a tsunami that struck the village of English Bay (now called Nanwalek), about 80 km east of the volcano (Davidson, 1884; Kienle and others, 1987; Siebert and others, 1995; Lander, 1996). Augustine is one of the most historically active volcanoes in the eastern Aleutian Arc (Simkin and Siebert, 1994; Miller and others, 1998), and its renewed eruptive activity in 2006 prompted concerns about a potential edifice collapse and subsequent tsunami.

During the 2006 eruption of Augustine, we performed a preliminary slope-stability analysis of the upper edifice. Numerous factors can affect the potential instability of volcanic edifices (Voight and Elsworth, 1997), including steep slopes, weakened rocks, strong earthquake shaking, shallow magma intrusion, elevated pore-fluid pressures induced by rain or snowmelt infiltration, or thermal fluid pressurization from intruding magma (Reid, 2004). Most of these factors are poorly known at Augustine as well as at other volcanoes. The 1883 edifice collapse occurred early in an eruption, and geologic evidence indicates the West Island debris avalanche occurred during an earlier eruption about 450 yr B.P., but it is uncertain whether all previous large slope failures were associated with eruptions. Rather than speculate on a myriad of destabilization scenarios, our preliminary analysis focused on two controls that are better known at Augustine: stresses

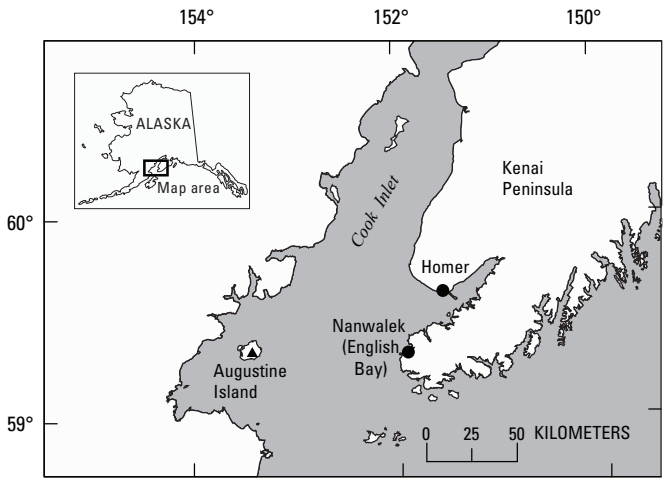

Figure 1. Southern Alaska, showing locations of Augustine Island, Cook Inlet, towns of Homer and Nanwalek (English Bay), and part of the Kenai Peninsula.

induced by topography and transient stresses created by strong ground motion during large earthquakes, in both of which rock strength strongly modulates potential slope instability. We used a quasi-three-dimensional (3D) geotechnical method implemented in the computer program SCOOPS (Reid and others, 2000) to perform our slope-stability assessments. We focused on potentially large (>0.1 km^3 volume) slope failures (landslides) affecting pre-2006 topography.

Herein we present a brief history of past debris avalanches from Augustine Volcano to provide a context for our slope-stability analyses, a short summary of our quasi-3D analytical approach, and the results for six plausible scenarios examining the effects of rock strength and earthquake-induced strong ground shaking at Augustine. Our preliminary analysis for each scenario indicates the relative stability of all parts of the upper edifice, the predicted least stable regions, and the volumes associated with potential slope failures.

History of Debris Avalanches at Augustine Volcano

Geologic studies on Augustine Island have identified and named at least 12 large debris-avalanche deposits on the flanks of the volcano that are younger than about 3,500 years (Waitt and others, 1996; Waitt and Begét, 2009; Waitt, this volume), each of which may have generated a tsunami when it flowed into Cook Inlet (Kienle and others, 1987; Begét and Kienle, 1992). Deposits of the West Island and Burr Point debris avalanches (fig. 2; table 1) possess the hummocky surface morphology, large megaclast blocks, and poorly sorted, fines-poor composition of similar deposits at Mount St. Helens (Siebert, 1984; Glicken, 1991). All of the large debris-avalanche deposits recognized on Augustine Volcano extend to the coast (Waitt and others, 1996; Waitt and Begét, 2009; Waitt, this volume) and typically are well exposed in seabluffs and gullies. Submerged hummocky topography offshore indicates that several of these debris avalanches traveled an additional 4 to 6 km across the sea floor.

Radiocarbon dating of buried soils associated with tephra and debris-avalanche deposits allowed Begét and Kienle (1992), Waitt and others (1996), and Waitt and Begét (2009) to propose a chronology for debris-avalanche formation at Augustine over the past 3,500 years (table 1). Their chronology is based on stratigraphic relations among dated tephra layers that are diagnostic enough in the field that they can be readily identified as stratigraphic markers. The stratigraphic relations of the debris-avalanche deposits to major tephra units can thus be used to establish age control on the debris-avalanche deposits. Other than the 1883 Burr Point deposit, no debris-avalanche deposits at Augustine have been directly dated, and it is unclear how many of these deposits are contemporaneous with major tephra units.

The spatial distribution of debris-avalanche deposits on Augustine Island indicates that debris avalanches have swept all sectors of the island in the past (fig. 2; table 1). At least five debris avalanches have occurred on the north and west flanks of the volcano, five on the east and south flanks, one on the northeast flank, and one on the southwest flank. The three most recent debris avalanches, including the 1883 Burr Point debris avalanche, postdate tephra B (about 478–257 yr B.P.) and have all been directed north-northwestward. Because of the approximately clockwise migration of slope failures around the edifice over the past several thousand years, some researchers have postulated an increased likelihood of future slope failure in the northeast sector (Siebert and Begét, 2006). The youngest debris avalanche on the southeast flank is recorded by the Southeast Beach debris-avalanche deposit (Waitt and Begét, 2009) which predates tephra B and postdates tephra M (about 709–478 yr B.P.).

Generalized physical descriptions of the debris-avalanche deposits at Augustine are presented by Waitt and others (1996) and Waitt and Begét (2009). Most of these deposits are composed of poorly sorted dacitic or andesitic rubble and silt- to boulder-size material. Megaclasts as large as 30 m across occur in some of the deposits; these clasts are intact pieces of former summit domes that were not disaggregated during downslope transport. Some of the clasts exhibit minor hydrothermal alteration, but only the Yellow Cliffs deposit (fig. 2) contains abundant material hydrothermally altered to clay. This debris-avalanche deposit is the only one at Augustine that records a flank collapse associated with pervasive alteration of the edifice.

Estimated volumes of the debris-avalanche deposits vary but most exceed 0.1 km^3. Siebert and others (1995) and Waitt and Begét (2009) estimated volumes for the debris-avalanche deposits on the north and west flanks of the volcano (table 1). The 1883 Burr Point debris-avalanche deposit has

Table 1. Characteristics of large debris-avalanche deposits on Augustine Island.

[Modified from Siebert and others (1995) and Waitt and Begét (2009). Composite stratigraphy includes debris-avalanche deposits and dated tephra deposits. Recalibrated radiocarbon ages (in years) bracketing tephras from Waythomas (2000)]

Composite stratigraphy	Map unit (fig. 2)	Sector of island affected	Volume of deposit (km^3)	Composition
Burr Point (A.D. 1883)	83a	North-northeast	0.25 to 0.3	Andesite, some alteration
Rocky Point	Bar	North	0.15	Andesite
West Island + Grouse Point	Baw, Bag	Northwest	0.3 to 0.5	Andesite, dacite
		(257±18) Tephra B (478±27)		
Southeast Beach	MBas	Southeast		Andesite
		(478±27) Tephra M (709±23)		
Lagoon	CMal	West		Andesite
		(709±23) Tephra C (1,102±22)		
North Bench	IMan	North-northwest		Andesite
Long Beach	HCal	Southwest		Andesite
South Point	HCas	South		Andesite
		(1,102±22) Tephra H (1,552±22)		
Northeast Point	IHa	Northeast		Andesite
		(1,552±22) Tephra I (1,736±26)		
Southeast Point	GIays	Southeast		Unaltered
Yellow Cliffs	GIays	Southeast		Andesite, extensive alteration
		(1,736±26) Tephra G (3,154±25)		
East Point	Ga	East		Andesite, some alteration

an estimated volume of 0.25 to 0.3 km^3; the missing volume of the edifice, resulting in a horseshoe-shaped crater, is about 0.24 km^3. Siebert and others (1995) suggested that multiple marginal levees and three depositional lobes resulted from an edifice failure which occurred in a retrogressive, closely timed process. The adjacent and underlying Rocky Point debris-avalanche deposit, which is only part exposed, has an estimated volume of 0.15 km^3, including its submarine extent. One of the largest edifice-failure events created the West Island debris-avalanche deposit, which has an approximate volume of 0.5 km^3. Older debris-avalanche deposits elsewhere on the island have patchy subaerial exposure, and most of them have submarine extents; volume estimates for these deposits are unavailable but probably range from 0.25 to 0.5 km^3.

Slope-Stability-Analysis Approach

To assess the future potential slope instability at Augustine Volcano, we use a quasi-3D, "method of columns" limit-equilibrium analysis that quantifies slope stability for different scenarios. Previously, we used this geotechnical approach to analyze the edifice stability at Mount St. Helens and Mount Rainier in Washington State (Reid and others, 2000; Reid and others, 2001) and at Volcán Casita in Nicaragua (Vallance and others, 2004), as well as on coastal bluffs in Seattle, Wash. (Brien and Reid, 2007). Our approach systematically searches the topography as defined by a digital elevation model (DEM) and computes the stability of millions of potential landslides affecting all parts of an edifice; these potential slope failures can encompass a wide range of depths and volumes. After this search is complete, every DEM gridpoint of interest will have been included in some potential landslides. The analysis results in maps portraying the relative stability of all parts of the edifice, the location of the overall least stable potential landslide, and the volumes of potential landslides. Our approach, implemented in the computer program SCOOPS, was detailed by Reid and others (2000) and is briefly described below.

At Augustine Volcano, we are interested in assessing the potential for massive flank collapse in places where the internal structure of the edifice is poorly known. For our analysis, we assumed arcuate potential failure surfaces. Although smaller rock failures are commonly controlled by local discontinuities, such as bedding or jointing surfaces, most large edifice collapses extend deep into the edifice, ignore smaller rock discontinuities, and create arcuate failure surfaces (Siebert, 1984; Voight and Elsworth, 1997). Potential failure surfaces composed of sections of a sphere represent the simplest 3D arcuate geometry unconstrained by internal discontinuities. We did not explicitly analyze the potential effects of internal discontinuities.

Each potential failure mass that we analyzed consists of a group of 3D vertical columns, as defined by the DEM, with a spherical failure surface at depth. Our method, which uses a 3D extension of Bishop's simplified method for two-dimensional rotational failure (Bishop, 1955), can incorporate variable 3D rock properties, 3D pore-fluid-pressure distributions, and simplistic earthquake-shaking effects. The shear resistance of each potential failure mass is given by the

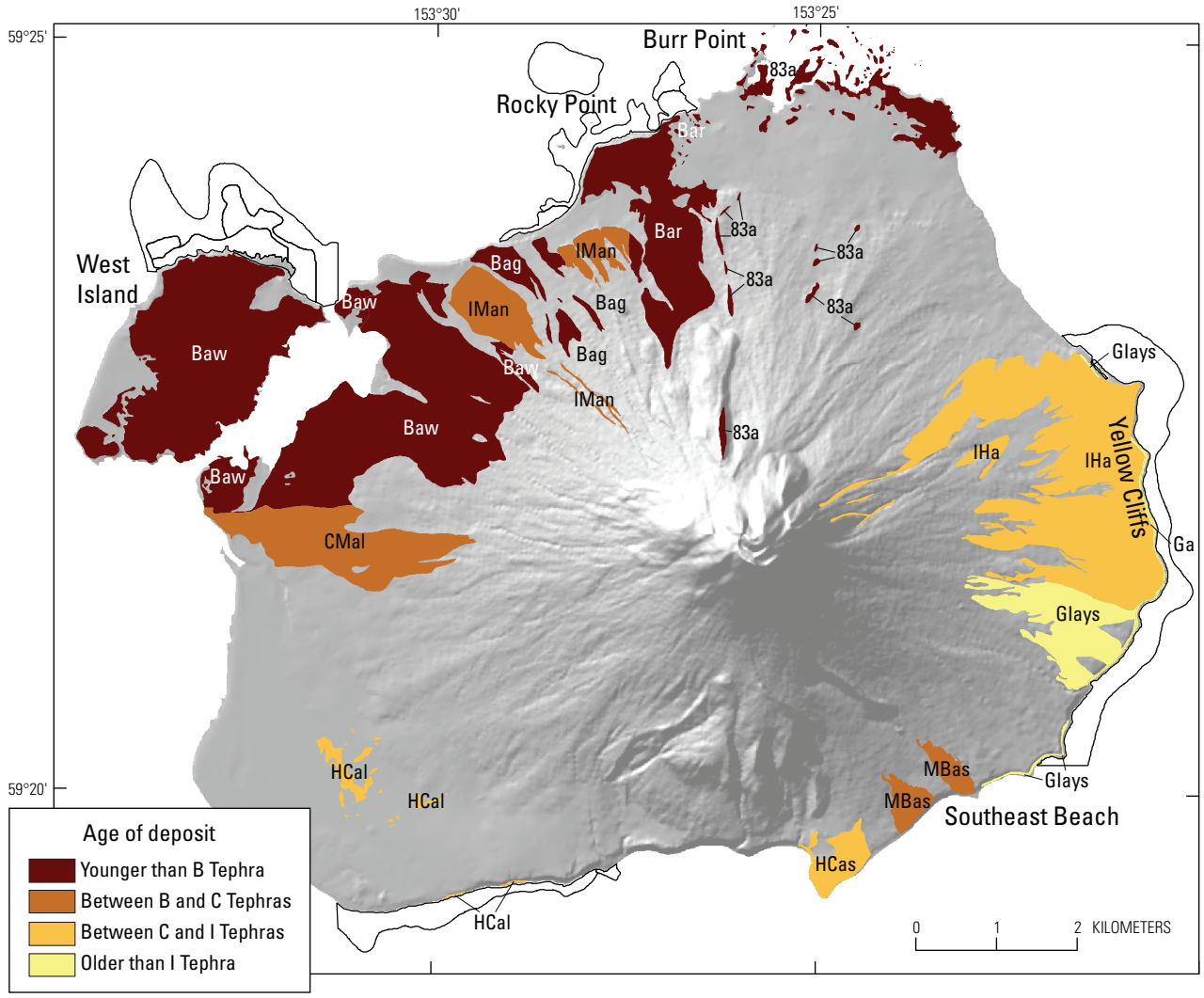

Figure 2. Augustine Island, showing distribution of large debris-avalanche deposits, grouped by age of separating tephra layers. Debris-avalanche unit names and mapped extent from Waitt and Begét (2009). Outlined areas nearshore show extent of some avalanche deposits. Debris-avalanche stratigraphy and tephra ages are listed in table 1. Except for Burr Point, local geographic names (for example, West Island, Rocky Point, Yellow Cliffs, and Southeast Beach) are informal. Shaded-relief image derived from U.S. Geological Survey 10-m digital elevation model (DEM) (unpub. data, 1990).

Coulomb-Terzaghi failure rule, $\tau = c + (\sigma_n - u)\tan\phi$, where c is the cohesion, σ_n is the total normal stress acting on the failure surface (a function of overlying rock weight), u is the pore-fluid pressure on the failure surface, and ϕ is the angle of internal friction. We compute a factor of safety, F, for each potential failure mass, using vertical-force equilibrium and rotational-moment equilibrium, as described by Reid and others (2000). Instability is reflected in F values <1.0; low F values indicate a propensity for collapse. This analysis accounts for the vertical stresses induced by topography and rock weight. We track the minimum F value affecting each DEM point and aggregate the results to produce factor-of-safety maps, as well as associated landslide volumes. If desired, destabilizing earthquake shaking can be incorporated as a pseudostatic horizontal force. Following the approach of Hungr (1987), this force is applied to the base of each vertical column in the potential failure mass (Reid and others, 2000).

Scenarios Analyzed for Augustine Volcano

For our preliminary slope-stability analysis, we need estimates of topography, rock properties (strengths and unit weights), and potential earthquake shaking. A water table at high elevations within the edifice could be destabilizing; such

a condition appeared to facilitate the 1980 collapse of Mount St. Helens (Voight and others, 1983). However, little is known about groundwater conditions at Augustine. Given fractured, permeable rocks in a generic edifice, groundwater-flow modeling suggests that an elevated water table is unlikely (Hurwitz and others, 2003), although localized perched groundwater or fluids in cracks could contribute to future edifice instability. Here, we ignore the possible effects of shallow magma intrusion or elevated pore-fluid pressures. We are interested in larger edifice failures and therefore analyze the stability of potential failures only of volumes from 0.1 to 1.0 km^3.

The pre-2006 topography of Augustine Island is well known, defined by a 10-m DEM derived from a 1:25,000-scale map (U.S. Geological Survey, unpub. data, 1990). A shaded-relief image of this DEM portraying local slope at each DEM node is shown in figure 3. Topographic modifications caused by the 2006 eruption had a relatively minor effect on the overall edifice geometry (fig. 4) and would likely have only minor effects on our analysis. Because we calculate the slope stability of massive failures encompassing large parts of the edifice, we resampled the DEM at a 50-m grid spacing for computational efficiency. For accurate estimates of F value and volume, about 100 DEM columns are needed to define each potential failure mass. Our resampled DEM spacing provides about 400 columns within potential failure masses near the low end of our desired volume range (0.1 km^3). Our search region for slope-stability analysis is limited to steeper sides of the volcanic edifice. Within this search region, we analyze the stability of millions of potential failure masses for each scenario.

A primary control on slope stability is shear strength. Rock properties, such as strength and unit weight, can vary drastically both spatially and temporally within a volcanic edifice. Fresh massive lava flows may be mechanically strong whereas air-fall deposits may be weak; even visually similar rock types may have spatially varying mechanical properties. Progressive acid sulfate-argillic hydrothermal alteration can weaken rocks over time, possibly promoting slope instability (Lopez and Williams, 1993; Watters and others, 2000; Reid and others, 2001).

The upper, steep part of Augustine Volcano is composed primarily of fresh andesite and dacite lava domes (fig. 4) with little or no visible hydrothermal alteration (Waitt and others, 1996; Waitt and Begét, 2009). Visual inspection by the

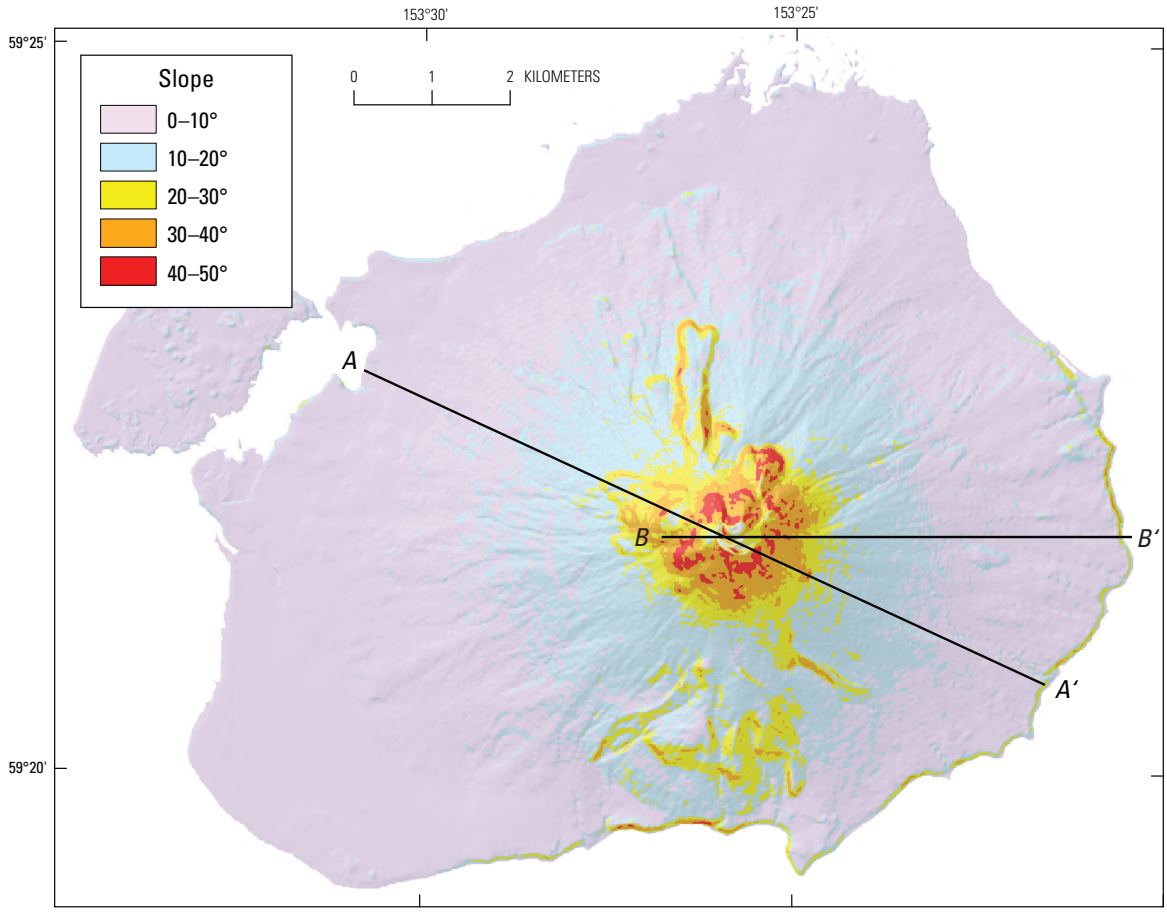

Figure 3. Augustine Island, showing slopes derived from unpublished U.S. Geological Survey (USGS) 10-m digital elevation model (DEM). Steepest slopes occur on upper edifice. Lines *A*–*A*′ and *B*–*B*′, locations of cross sections in figures 4 and 7. Shaded-relief image derived from U.S. Geological Survey 10-m digital elevation model (DEM) (unpub. data, 1990).

first author of the upper domes in 1997 also revealed only localized alteration at fumaroles. Thus, the carapace of the modern Augustine edifice appears to lack widespread acid sulfate alteration. This style of alteration, present at Mount Rainier (Finn and others, 2001), can weaken rocks (Watters and others, 2000) and significantly reduce slope stability (Reid and others, 2001). The upper Augustine edifice, composed primarily of fresh dome rocks, is more nearly uniform than in the notable layering at some other stratovolcanoes. Although nearly all the debris-avalanche deposits derived from the Augustine edifice contain little altered rock, the Yellow Cliffs deposit does contain hydrothermally altered clay. Thus, more altered rocks may be present at depth within the edifice.

For our preliminary slope-stability analysis, we use two end-member scenarios, assuming uniform shear strength (defined by internal angle of friction and cohesion) and unit weight (table 2), representing strong rocks and relatively weak altered rocks. No direct measurements of strength or unit weight are known for Augustine Volcano dome rocks. Cohesion can play a crucial role in defining the volume and depth of a slope failure (Reid and others, 2000), but estimating the cohesion of rocks at depth within an edifice is difficult. Solid, dense igneous rocks can have a cohesion of 10,000 to 100,000 kPa, but highly altered rocks only 10 kPa. Using either surface-rock exposures or debris-avalanche deposits from volcanoes, other researchers have obtained a few measurements of cohesion and internal angle of friction, including at Mount St. Helens (Voight and others, 1983), Mounts Rainier and Hood (Watters and others, 2000), and Citlaltépetl (Zimbelman and others, 2004). We used these published strength values from volcanoes, as well as values determined for other igneous rocks (Jaeger and Cook, 1979; Hoek and Bray, 1981), to constrain our estimates of shear strength. Our end-member scenarios likely bracket values within the Augustine edifice, although Augustine dome rocks probably have properties closer to those of strong rocks (table 2). Rock properties likely vary within the Augustine edifice. Nevertheless, these end members illustrate the possible effects on slope instability.

Finally, we analyzed several scenarios involving large earthquakes. Augustine Island is subject to large tectonic earthquakes with probable ground motions much greater than those of local volcanic or volcano-tectonic origin. Other researchers have estimated probable peak ground accelerations (PGAs) throughout Alaska by combining frequency and magnitude estimates of earthquakes from potential sources with empirical relations for strong-ground-motion attenuation with distance from the source (Wesson and others, 2007). This method estimates strong ground motion for various probabilities of earthquake occurrence. In Alaska, the method takes into account fault sources, such as the Alaska-Aleutian megathrust, and the available seismic record (Wesson and others, 2007). Estimated PGA values are high in much of southern Alaska. From results derived for the Augustine Island region, we selected two PGA values to bracket potential moderate to large earthquakes at Augustine, where a PGA value of 0.35 *g* corresponds to about a 10-percent probability of exceedance in 50 years and a PGA value of 0.5 *g* corresponds to about a 2-percent probability of exceedance in 50 years. As discussed above, these estimated accelerations can be treated as a pseudostatic horizontal force in our analyses. We follow the approach that Voight and others (1983) applied at Mount St. Helens and use the same strength parameters in our ground-shaking scenarios as in our static scenarios. The combination of a static scenario and two ground-shaking scenarios for both strong and weak edifice rocks produces the six scenarios listed in table 2.

Results of Simulations

The minimum stabilities computed by using the program SCOOPS for the six scenarios listed in table 2 are mapped in figure 5, representing the lowest *F* values computed for any potential landslide encompassing each DEM node. Potential landslides with the lowest *F* values are defined as critical failures. The outline of the overall least stable potential landslide (out of about 20 million) computed for each scenario is also shown in figure 5. These results do not necessarily show complete failure masses, except for the overall minimum outlined in black, nor do they indicate that areas with similar *F* values will fail simultaneously. The computed volumes within the target range 0.1 to 1.0 km^3 associated with the least stable

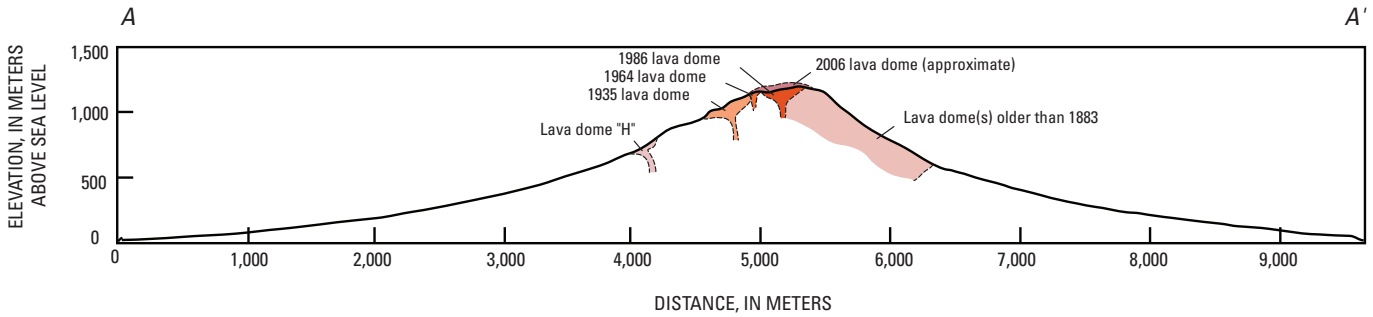

Figure 4. Geologic cross section *A*–*A*′ through Augustine Volcano (see fig. 3 for location), showing dome rocks in upper edifice. Geologic units modified from Waitt and others (1996), with approximate location of 2006 dome added. No vertical exaggeration.

Table 2. Slope-stability scenarios analyzed for Augustine Volcano.

[*F*, factor of safety; PGA, peak ground acceleration]

Scenario	Input				Results	
	Friction angle (°)	Cohesion (kPa)	Unit weight (kN/m³)	Earthquake PGA (*g*)	Minimum *F*	Volume of minimum *F* mass (km³)
1	40	1,000	24	0	2.42	0.13
2	40	1,000	24	0.35	1.35	0.17
3	40	1,000	24	0.5	1.10	0.21
4	28	300	21	0	1.29	0.10
5	28	300	21	0.35	0.71	0.11
6	28	300	21	0.5	0.57	0.11

potential landslide (critical failure) at each DEM node are shown in figure 6. By selecting a point in figure 5, the associated volume can be determined in figure 6.

Variations in potential slope stability induced by differences in rock strength within the Augustine edifice are illustrated in figures 5*A* (uniformly strong rocks) and 5*D* (uniformly weak rocks). These results indicate that (1) a strong-rock edifice has much higher *F* values (min 2.42), whereas a weak-rock edifice has *F* values approaching 1, the limit of stability; (2) the predicted least stable potential landslide is on the upper east flank in both scenarios; and (3) most of the steep upper edifice has *F* values like those of the least stable mass in both scenarios. In these scenarios, potential large landslides have an approximately equal likelihood of initiating from any side of the edifice. Volumes associated with the least stable mass are close to the lower volume limit of 0.1 km³ in both scenarios (figs. 6*A*, 6*D*).

The potentially destabilizing effects of earthquake ground shaking on the Augustine edifice are illustrated in figures 5*B*, 5*C*, 5*E*, and 5*F*. Given a uniformly strong edifice, moderate ground shaking (PGA value, 0.35 *g*) reduces the *F* value throughout the edifice (fig. 5*B*), but the pattern of stability is similar to that of the non-earthquake scenario (fig. 5*A*). In this scenario, the least stable potential landslide (*F* value, 1.35) is still on the east flank, and most of the upper edifice has similar *F* values. Strong ground shaking (PGA value, 0.5 *g*) further reduces the minimum *F* value almost to 1, and the predicted least stable mass is on the east flank. An interesting effect is shown by the increases in volume and depth associated with the least stable potential landslide (fig. 7; table 2): with strong rocks, the least stable volume increases from 0.13 km³ with no shaking, through 0.17 km³ with moderate shaking, to 0.21 km³ with strong shaking.

Given a uniformly weak edifice, *F* values throughout the edifice also decrease with increasing ground shaking (compare figs. 5*D* through 5*F*). As with the strong-rock scenarios, the overall pattern of *F* values remains similar between scenarios. Much of the upper edifice has similar *F* values, and the least stable potential landslide is on the east flank. However, absolute *F* values are considerably lower, and computed minimum *F* values are well below 1 in both the moderate- and strong-ground shaking scenarios (figs. 5*E*, 5*F*; table 2). A pseudostatic-force analysis using peak ground accelerations often produces lower calculated *F* values; therefore, instability can be exaggerated (Seed, 1973; Chowdhury, 1978). In these weak-rock scenarios, all the computed volumes associated with the least stable potential landslides are close to the lower limit of 0.1 km³, suggesting that our preset lower volume limit is controlling the predicted sizes of landslides, rather than are edifice geometry and material properties.

Discussion

The results of our simulations of Augustine edifice stability highlight the effects of topography in controlling the location of potential future slope instability. Large-volume failures integrate destabilizing effects over many DEM nodes. Thus, our maps of calculated slope stability (fig. 5) differ somewhat from a map of local slope at the DEM nodes (fig. 3). Large areas of steep local slope occur on the north and northwest flanks of the edifice (fig. 3), whereas our results indicate that the east flank is potentially the least stable. The relatively small north-northwest-facing theater at the current summit does not appear to exert a strong control on the location of potential large edifice failures. Our results also indicate that most of the steep, upper edifice has similar stabilities for a given scenario, as might be expected for a relatively symmetric cone. This result suggests that in the absence of locally destabilizing events, an approximately equal likelihood exists of a future slope failure affecting any sector of the volcano. Such results agree well with the observation that past debris avalanches have inundated all sectors of the island (Begét and Kienle, 1992; Waitt and Begét, 2009).

Most of the scenarios that we evaluated predict a stable edifice. Parts of the edifice are predicted to become unstable only in scenarios that involve extensive weak, possibly hydrothermally altered rocks and moderate to severe ground shaking. Because Augustine rock strengths are likely nearer those

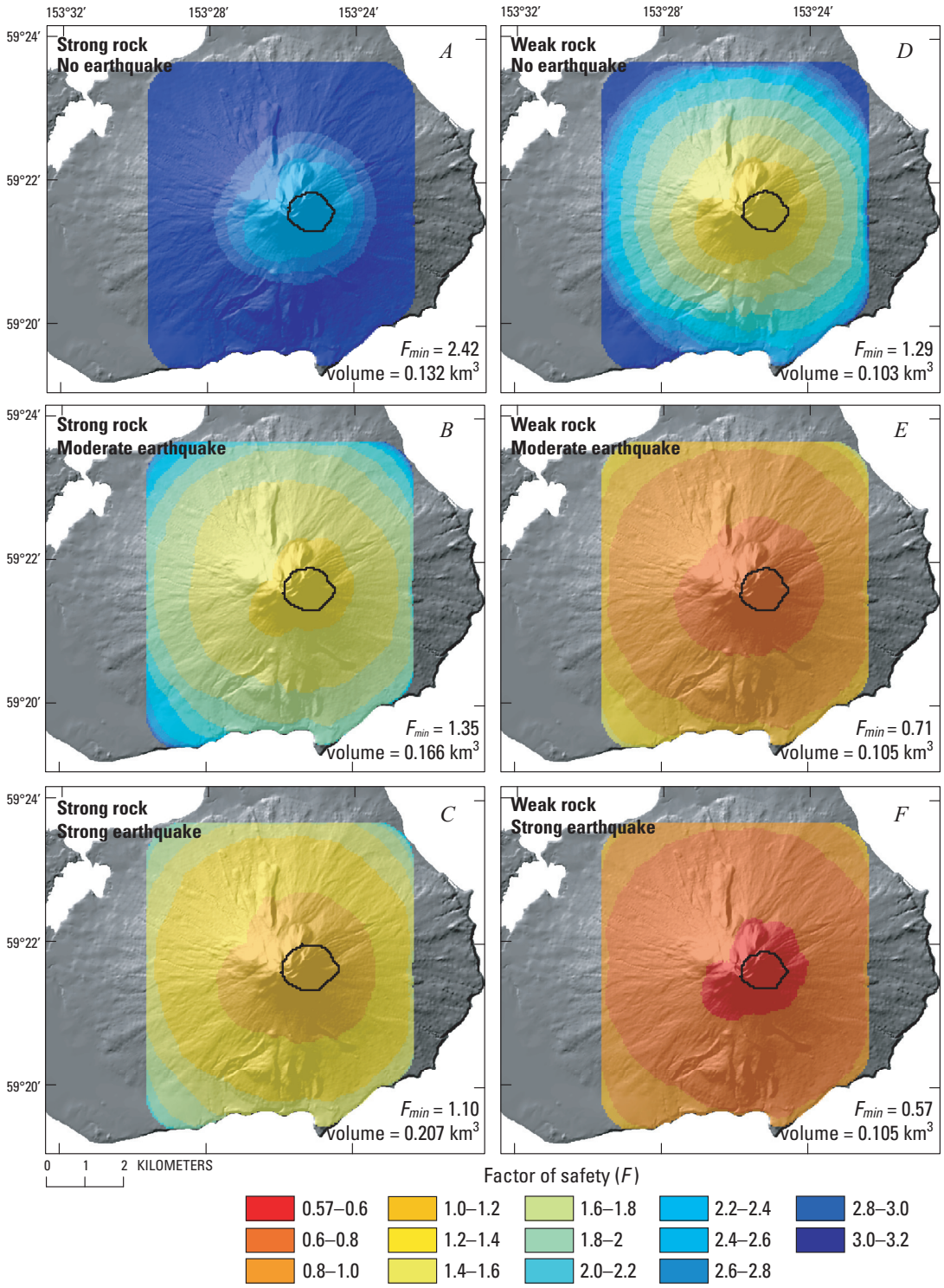

Figure 5. Augustine Volcano, showing computed slope stability of the edifice for six scenarios listed in table 2. Lowest computed factor of safety (*F*) for any potential landslide intersecting each digital elevation model (DEM) node (critical failure) is shown for area searched in our analysis. Warmer colors indicate lower stability; orange and red areas are potentially unstable. Black outline, area of predicted overall least stable potential landslide; minimum factor of safety (F_{min}) and volume associated with this potential landslide are denoted on each diagram. *A*, Scenario 1, with strong rock and no earthquake ground shaking. *B*, Scenario 2, with strong rock and moderate earthquake ground shaking. *C*, Scenario 3, with strong rock and strong earthquake ground shaking. *D*, Scenario 4, with weak rock and no earthquake ground shaking. *E*, Scenario 5, with weak rock and moderate earthquake ground shaking. *F*, Scenario 6, with weak rock and strong earthquake ground shaking. Shaded-relief image derived from U.S. Geological Survey 10-m digital elevation model (DEM) (unpub. data, 1990).

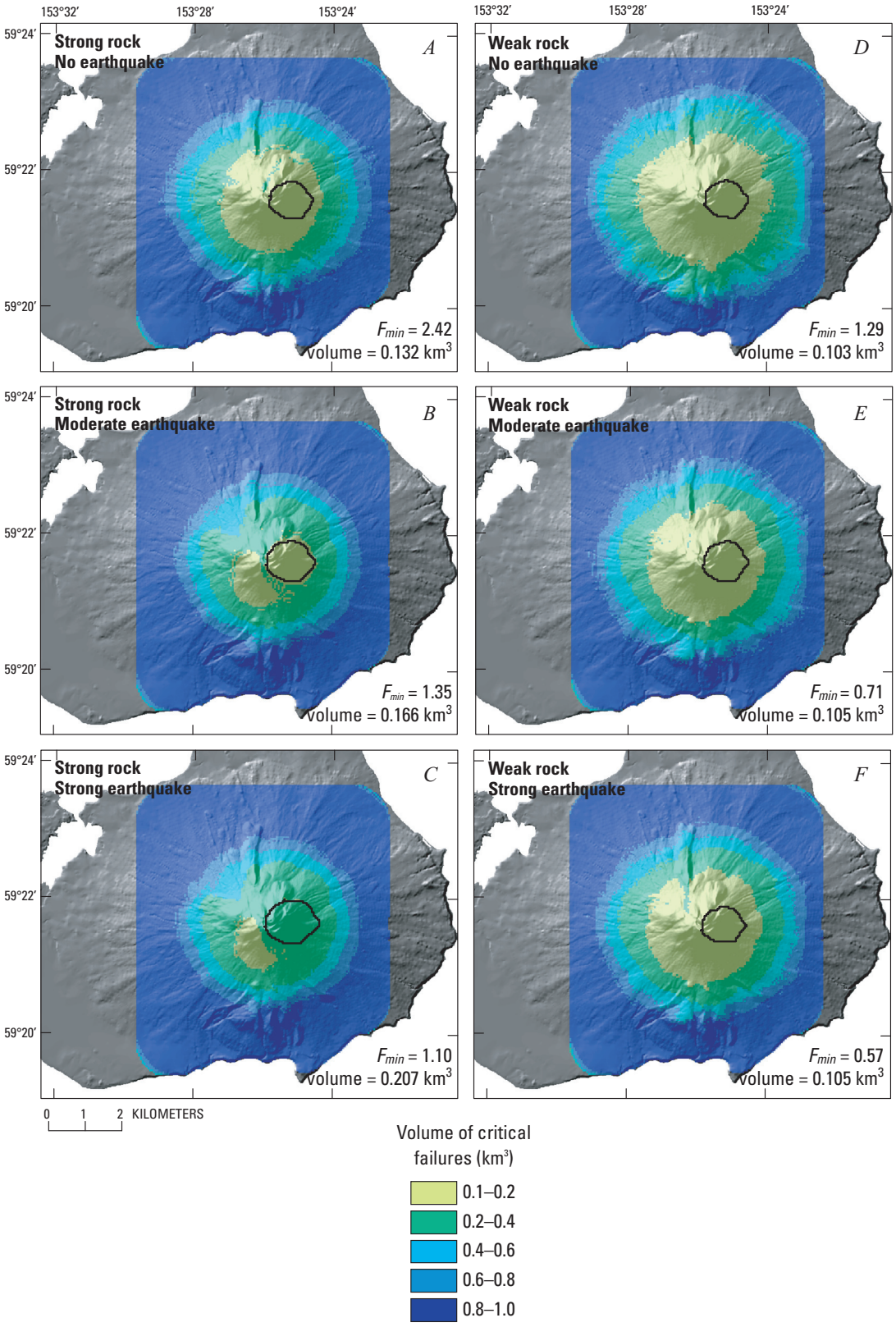

Figure 6. Augustine Volcano, showing potential landslide volumes associated with computed stability of critical failures shown in figure 5. Black outline, area of predicted least stable potential landslide. Six scenarios (*A*-*F*) shown are summarized in figure 5 and listed in table 2. Shaded-relief image derived from U.S. Geological Survey 10-m digital elevation model (DEM) (unpub. data, 1990). See figure 5 for explanation of abbreviations.

of strong rocks, our results suggest that the edifice is unlikely to undergo a massive landslide triggered solely by gravitational failure or a moderate earthquake. Even in scenarios with pervasive weak rocks, slopes are unlikely to fail by gravity alone (fig. 5*D*), implying that additional triggering mechanisms, such as shallow magma intrusion, local oversteepening caused by deformation, and (or) thermal pressurization of pore fluids or gases, are needed to provoke massive collapse at Augustine Volcano.

Although predicted least stable landslide volumes in most of our scenarios are near the lower limit of 0.1 km^3, this analysis does not directly account for retrogressive failure, as occurred at Mount St. Helens in 1980 (Voight and others, 1983; Voight and Elsworth, 1997). At Mount St. Helens, a retrogressive style of collapse increased the failure volume from about 0.8 km^3 for the initial slide block to 2.3 km^3 for all three slide blocks (Voight and others, 1983; Reid and others, 2000). In addition, failed rock masses typically expand as they move downslope. At Mount St. Helens, the volume increased from 2.3 km^3 of source rock to about 2.8 km^3 of debris-avalanche deposit (Voight and others, 1983). At Augustine, both failure retrogression and dilation of debris could enlarge a debris avalanche from its initial failure volume. Stress changes in the subsurface induced by shallow magma intrusion or thermal pressurization could also instigate a larger initial landslide.

A future edifice collapse that produces a debris avalanche with a volume >0.1 km^3 would likely reach the ocean and could generate a tsunami. Our preliminary results suggest that the likelihood of collapse is nearly equal on all sides of the island, although the travel distance from source to coast varies around the island. However, our results indicate that the east flank is marginally less stable. Any avalanche from this flank would travel into deep water, which can enhance the formation of larger tsunamis (Waythomas and others, 2006). A tsunami generated on this side of the island would be directed more toward the southwestern part of the Kenai Peninsula (fig. 1) and the town of Homer (~110 km away) than would a tsunami initiated on the north (as in 1883) or west side of the island.

This preliminary slope-stability analysis focuses primarily on the effects of topography and earthquake shaking. It does not account for spatially varying rock properties within the edifice, the occurrence of such dynamic triggers as shallow magma intrusion or thermal pressurization, or potential retrogression of an initial failure into the edifice. Also, we did not evaluate possible changes in slope stability induced by new lava-dome growth during the 2006 eruption. Nevertheless, our results highlight potential failure locations, given reasonable assumptions about the Augustine edifice. With additional research, rock properties might be better defined, although determining them for rocks at potential failure depth deep within the edifice would be difficult. Possible dynamic triggering events might also be better modeled. Future instability at Augustine Volcano will likely be accompanied by volcanic unrest. Monitoring seismicity and ground deformation should aid in detecting shallow magma movement and may help in short-term forecasting of impending edifice failure.

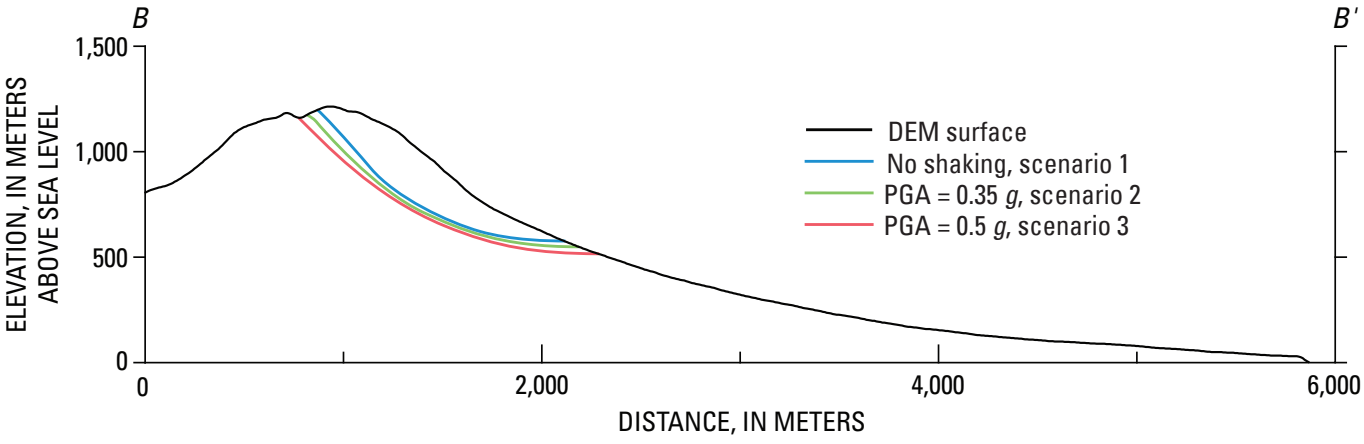

Figure 7. Cross section *B–B′* through Augustine Volcano (see figure 3 for location), showing predicted least stable potential landslide surfaces for scenarios 1 (no earthquake shaking), 2 (moderate ground shaking with peak ground acceleration = 0.35 *g*), and 3 (strong ground shaking with peak ground acceleration = 0.5 *g*), all with strong rocks. Volume of predicted least stable landslide increases with increasing strength of ground shaking (table 2). No vertical exaggeration. DEM, digital elevation model; PGA, peak ground acceleration.

References Cited

Begét, J.E., Gardner, C., and Davis, K., 2008, Volcanic tsunamis and prehistoric cultural transitions in Cook Inlet, Alaska: Journal of Volcanology and Geothermal Research, v. 176, p. 377–386.

Begét, J.E., and Kienle, J., 1992, Cyclic formation of debris avalanches at Mount St. Augustine volcano: Nature, v. 356, no. 6371, p. 701–704.

Begét, J.E., and Kowalik, Z., 2006, Confirmation and calibration of computer modeling of tsunamis produced by Augustine Volcano, Alaska: Science of Tsunami Hazards, v. 24, no. 4, p. 257–266.

Bishop, A.W., 1955, The use of slip circles in the stability analysis of slopes: Geotechnique, v. 5, p. 7–17.

Brien, D.L., and Reid, M.E., 2007, Modeling 3-D slope stability of coastal bluffs using 3-D ground-water flow, southwestern Seattle, Washington: U.S. Geological Survey Scientific Investigations Report 2007-5092, 54 p. [http://pubs.usgs.gov/sir/2007/5092/].

Chowdhury, R.N., 1978, Slope analysis: Amsterdam, Elsevier, v. 22, 423 p.

Davidson, G., 1884, Notes on the volcanic eruption of Mount Saint Augustine, Alaska, October 6, 1883: Science, v. 3, no. 54, p. 186–189.

Finn, C.A., Sisson, T.W., and Deszcz-Pan, M., 2001, Aerogeophysical measurements of collapse-prone hydrothermally altered zones at Mount Rainier volcano: Nature, v. 409, p. 600–603.

Glicken, H., 1991, Sedimentary architecture of large volcanic-debris avalanches, *in* Fisher, R.V., and Smith, G.A., eds., Sedimentation in volcanic settings: Santa Barbara, Calif., Society of Economic Paleontologists and Mineralogists, p. 99–106.

Hoek, E., and Bray, J.W., 1981, Rock slope engineering (3d ed.): London, Institute of Mining and Metallurgy, 358 p.

Hungr, O., 1987, An extension of Bishop's simplified method of slope stability analysis to three dimensions: Geotechnique, v. 37, no. 1, p. 113–117.

Hurwitz, S., Kipp, K.L., Ingebritsen, S.E., and Reid, M.E., 2003, Groundwater flow, heat transport, and water table position within volcanic edifices—Implications for volcanic processes in the Cascade Range: Journal of Geophysical Research, v. 108, no. B12, DOI: 10.1029/2003JB002565.

Jaeger, J.C., and Cook, N.G.W., 1979, Fundamentals of rock mechanics (3d ed.): New York, Chapman and Hall, 593 p.

Kienle, J., Kowalik, Z., and Murty, T.S., 1987, Tsunamis generated by eruptions from Mount St. Augustine volcano, Alaska: Science, v. 236, no. 4807, p. 1442–1447.

Kienle, J., and Swanson, S.E., 1985, Volcanic hazards from future eruptions of Augustine Volcano, Alaska (2d ed.): Fairbanks, University of Alaska, Geophysical Institute Report UAG-R 275, 122 p.

Lander, J.F., 1996, Tsunamis affecting Alaska: Boulder, Colo., U.S. National Oceanic and Atmospheric Administration, National Environmental Satellite Data and Information Service, National Geophysical Data Center, 195 p.

Lopez, D.L., and Williams, S.N., 1993, Catastrophic volcanic collapse; relation to hydrothermal processes: Science, v. 260, no. 5115, p. 1794–1796.

Miller, T.P., McGimsey, R.G., Richter, D.H., Riehle, J.R., Nye, C.J., Yount, M.E., and Dumoulin, J.A., 1998, Catalog of the historically active volcanoes of Alaska: U.S. Geological Survey Open-File Report 98-0582, p. 104.

Reid, M.E., 2004, Massive collapse of volcano edifices triggered by hydrothermal pressurization: Geology, v. 32, no. 5, p. 373–376.

Reid, M.E., Christian, S.B., and Brien, D.L., 2000, Gravitational stability of three-dimensional stratovolcano edifices: Journal of Geophysical Research, v. 105, no. B3, p. 6043–6056.

Reid, M.E., Sisson, T.W., and Brien, D.L., 2001, Volcano collapse promoted by hydrothermal alteration and edifice shape, Mount Rainier, Washington: Geology, v. 29, no. 9, p. 779–782.

Seed, H.B., 1973, Stability of earth and rockfill dams during earthquakes, *in* Hirshfeld, R.C., and Poulos, S.J., eds., Embankment-dam engineering: New York, Wiley and Sons, p. 239–269.

Siebert, L., 1984, Large volcanic debris avalanches; characteristics of source areas, deposits, and associated eruptions: Journal of Volcanology and Geothermal Research, v. 22, p. 163–197.

Siebert, L., and Begét, J.E., 2006, Two millennia of edifice instability at Augustine Volcano, Alaska and implications for future collapse: Eos, American Geophysical Union Transactions, v. 87, no. 52, fall meeting supp., abstract V51C-1692.

Siebert, L., Begét, J.E., and Glicken, H., 1995, The 1883 and late-prehistoric eruptions of Augustine volcano, Alaska: Journal of Volcanology and Geothermal Research, v. 66, p. 367–395.

Siebert, L., Glicken, H., and Kienle, J., 1989, Debris avalanches and lateral blasts at Mount St. Augustine volcano, Alaska: National Geographic Research, v. 5, no. 2, p. 232–249.

Simkin, T., and Siebert, L., 1994, Volcanoes of the world (2d ed.): Tucson, Ariz., Geoscience Press, 349 p.

Vallance, J.W., Schilling, S.P., Devoli, G., Reid, M.E., Howell, M.M., and Brien, D.L., 2004, Lahar hazards at Casita and San Cristóbal Volcanoes, Nicaragua: U.S. Geological Survey Open-File Report 2001-468, 18 p., 3 map plates.

Voight, B., and Elsworth, D., 1997, Failure of volcano slopes: Geotechnique, v. 47, no. 1, p. 1–31.

Voight, B., Janda, R.J., Glicken, H., and Douglass, P.M., 1983, Nature and mechanics of the Mount St. Helens rockslide-avalanche of 18 May 1980: Geotechnique, v. 33, p. 243–273.

Waitt, R.B., 2010, Ejecta and landslides from Augustine Volcano before 2006, *in* Power, J.A., Coombs, M.L., and Freymueller, J.T., eds., The 2006 eruption of Augustine Volcano, Alaska: U.S. Geological Survey Professional Paper 1769 (this volume).

Waitt, R.B., and Begét, J.E., 2009, Volcanic processes and geology of Augustine Volcano, Alaska: U.S. Geological Survey Professional Paper 1762, 78 p., 2 map plates, [http://pubs.usgs.gov/pp/1762].

Waitt, R.B., Begét, J.E., and Kienle, J., 1996, Provisional geologic map of Augustine Volcano, Alaska: U.S. Geological Survey Open-File Report 96-516, 44 p., 1 map plate.

Watters, R.J., Zimbelman, D.R., Bowman, S.D., and Crowley, J.K., 2000, Rock mass strength assessment and significance to edifice stability, Mount Rainier and Mount Hood, Cascade Range Volcanoes: Pure and Applied Geophysics, v. 157, p. 957–976.

Waythomas, C.F., 2000, Reevaluation of tsunami formation by debris avalanche at Augustine Volcano, Alaska: Pure and Applied Geophysics, v. 157, p. 1145–1188.

Waythomas, C.F., and Waitt, R.B., 1998, Preliminary volcano-hazard assessment for Augustine Volcano, Alaska: U.S. Geological Survey Open-File Report 98-0106, 39 p.

Waythomas, C.F., Watts, P., and Walder, J.S., 2006, Numerical simulation of tsunami generation by cold volcanic mass flows at Augustine Volcano, Alaska: Natural Hazards and Earth System Sciences, v. 6, p. 671–685.

Wesson, R.L., Boyd, O.S., Mueller, C.S., Bufe, C.G., Frankel, A.D., and Petersen, M.D., 2007, Revision of time-independent probabilistic seismic hazard maps for Alaska: U.S. Geological Survey Open-File Report 2007–1043, 33 p.

Zimbelman, D.R., Watters, R.J., Firth, I.R., Breit, G.N., and Carrasco-Núñez, G., 2004, Stratovolcano stability assessment methods and results from Citlaltépetl, Mexico: Bulletin of Volcanology, v. 66, no. 1, p. 66–79.